Transport and spin conversion of multicarriers in semimetal bismuth

Hiroyuki Emoto,[1,2] Yuichiro Ando,[1] Gaku Eguchi,[1,3] Ryo Ohshima,[1,2] Eiji Shikoh,[4] Yuki Fuseya,[5] Teruya Shinjo,[1] and Masashi Shiraishi[1,*]

[1]*Department of Electronic Science and Engineering, Kyoto University, Nishikyo-ku, Kyoto, 615-8510, Japan*

[2]*Graduate School of Engineering Science, Osaka University, Toyonaka, Osaka 560-8530, Japan*

[3]*Institute of Solid State Physics, TU-Wien, 1040 Vienna, Austria*

[4]*Graduate School of Engineering, Osaka City University, Sumiyoshi-ku, Osaka, 558-8585, Japan*

[5]*Department of Engineering Science, University of Electro-Communications, Chofu, Tokyo 182-8585, Japan*

(Received 24 January 2016; revised manuscript received 9 May 2016; published 31 May 2016)

In this paper, we report on the investigation of (i) the transport properties of multicarriers in semimetal Bi and (ii) the spin conversion physics in this semimetal system on a ferrimagnetic insulator, yttrium-iron-garnet. Hall measurements reveal that electrons and holes coexist in the Bi, with electrons being the dominant carrier. The results of a spin conversion experiment corroborate the results of the Hall measurement; in addition, the inverse spin Hall effect governs the spin conversion in the semimetal/insulator system. This study provides further insights into spin conversion physics in semimetal systems.

DOI: 10.1103/PhysRevB.93.174428

I. INTRODUCTION

Semimetal bismuth (Bi) is one of the most intensively studied elements in solid-state physics, and a wide variety of attractive physics, such as the Nernst-Ettingshausen effect [1], the Shubnikov–de Haas oscillation [2], the de Haas–van Alphen effect [3], the Seebeck effect [4], and so on, has been discovered by using Bi. Studies of Bi in solid-state physics [5] have demonstrated that the low-energy effective Hamiltonian of Bi is given by the Dirac Hamiltonian with a small band gap (approximately 10 meV) at the L-point [6–8], strong diamagnetism [9], and a large spin-orbit interaction (SOI, approximately 1.8 eV) [10]. Meanwhile, difficulty in spin injection, resulting in spin transport, in Bi has impeded exploration of spin-related physics in Bi. However, recently, spin-related physics, i.e., spin transport and a spin-to-charge conversion effect (and its reciprocal effect), in Bi has been attracting strong attention. Spin-related physics can provide a new aspect in Bi physics because a new spin-injection method, spin pumping, has been established [11–14]. The correlation between a possible long momentum relaxation length, due to the Dirac-like linear band structure, and the quite large SOI, resulting in rapid spin relaxation, attracts strong attention in spintronics because these properties govern spin transport and spin conversion in Bi. Electric spin conversion is the conversion from an electric current to a spin current and *vice versa*, such as the spin Hall effect and the inverse spin Hall effect (ISHE). Here, the spin carrier species, i.e., electrons or holes, govern the sign of the electromotive forces generated by the ISHE. Charge transport properties in a semimetal system such as Bi, where electrons and holes coexist, can be understood from the longitudinal and transverse resistivity, and a recent relevant analysis enables further insight into the multicarrier transport [15]. Hence, a combination of electric spin conversion and resistivity measurements enables greater understanding of the physics involving the correlation between spin and charge transport in semimetals. An example of the experimental demonstration of spin conversion in Bi is the ISHE [11,12], and these studies are motivated by the large SOI of Bi. Another notable study is the inverse Rashba-Edelstein effect (IREE) [13,14] appearing at a Bi/Ag interface, which has been attributed to large Rashba splitting at the interface [16]. However, further discussion of the spin conversion physics that considers multicarrier transport in Bi remains lacking.

The purpose of this study is to investigate spin and charge transport and their conversion in Bi via Hall and ISHE measurements, where the former enables investigation of charge transport and the latter enables the study of spin transport and its conversion properties. We chose a Bi/yttrium-iron-garnet (YIG) heterostructure, in which the Bi deposited on the YIG is polycrystalline. The introduction of the magnetic insulator YIG, instead of a conductive ferromagnetic metal such as NiFe, enables us to bypass the problem of the superposition of unwanted electromotive forces under ferromagnetic resonance (FMR) from the conductive ferromagnet on the spin conversion signals [17,18]. In addition, the semimetal/insulator interface can induce the Rashba field, which enables detection of the IREE.

II. EXPERIMENTS

Bi thin films were fabricated on single crystalline YIG, where the thickness of the Bi was varied from 5 to 60 nm. Figure 1(a) shows an x-ray diffraction θ-2θ pattern of the Bi sample (20 nm thick), where Cu-Kα radiation was used. The peaks labeled (003), (006), and (009) were observed, whereas the peaks labeled (012) and (110) were not. This directly implies that (001) is the preferential orientation. By contrast, the appearance of the (104) peak indicates that the Bi is not perfectly aligned to the (001) direction. This result tells us that (i) 80% of the Bi is polycrystalline and that (ii) the Bi is rhombohedral and oriented along (001) with 20% of the (104)-oriented crystal. In order to estimate the grain size of Bi, we carried out atomic force microscopy (AFM) measurements of the Bi thin film (60 nm thick). Figure 1(b) shows an AFM image of the Bi, and a typical grain size is several hundreds of nanometers. Electric

*Corresponding author: mshiraishi@kuee.kyoto-u.ac.jp

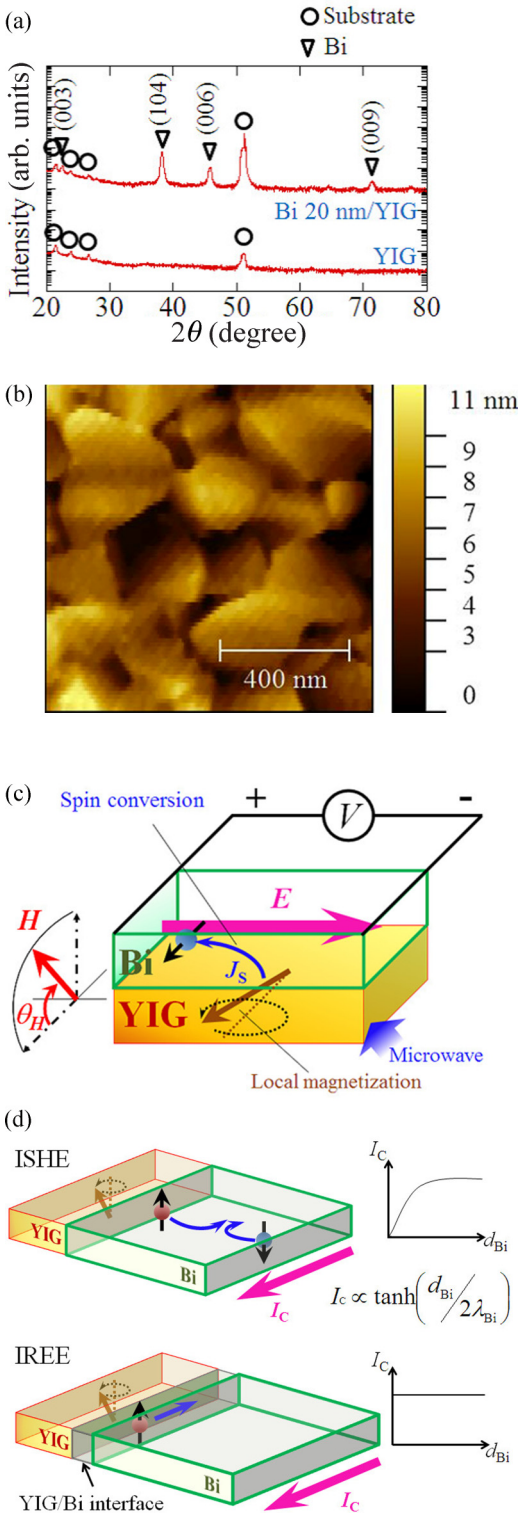

FIG. 1. (a) X-ray diffraction patterns of Bi (20 nm)/YIG and of YIG. The crystalline peaks are identified as shown in the figure. (b) An atomic force microscopic view of the Bi. (c) Schematic image of the spin conversion device. θ_H is the angle of an external magnetic field, H, to the YIG plane. (d) Illustration of different spin conversion principles in the ISHE and the IREE.

transport properties of the Bi/YIG film were determined using the conventional four-probe technique with a commercial apparatus (Quantum Design PPMS). Electrical contacts were made using room-temperature-cured silver paste, and the process was performed under atmospheric conditions. The measurement was implemented in the temperature range of 30 to 300 K to investigate charge carrier transport properties, and the thickness of the Bi varied from 8 to 70 nm. We introduced spin pumping to inject a pure spin current from the YIG to the Bi to study the spin-to-charge conversion physics in this semimetal. Spin pumping is a method of spin injection from a ferromagnet/ferrimagnet to a nonmagnet under FMR of the ferromagnet/ferrimagnet. Under FMR, spin angular momenta in the ferromagnet/ferrimagnet are transferred to the conducting electrons in the nonmagnet via *s-d* coupling, resulting in spin accumulation and generation of a pure spin current in the nonmagnet [19]. In the spin pumping measurements, the Bi/YIG sample was placed in a nodal position of a TE_{011} (transverse electric mode) cavity of an electron spin resonance (ESR) system (JEOL FA-200), where the alternating electric and magnetic field components were at a minimum and a maximum, respectively (the microwave frequency was set to be 9.12 GHz). The excitation power of the microwave was applied up to 1 mW. An external static magnetic field for obtaining the FMR was applied at an angle, θ_H, as shown in Fig. 1(c). All measurements of the spin pumping were performed at room temperature (RT).

In order to distinguish the ISHE and the IREE in the Bi/YIG, the Bi thickness dependence of a generated electric current provides important information. As illustrated in Fig. 1(d), the physical origins of the ISHE and the IREE are essentially different. In the ISHE, spin-dependent scattering gives rise to conversion of a spin current to a charge current, and the length scale of the conversion is determined by the spin diffusion length. Hence, the thickness dependence of the generated charge current exhibits a characteristic behavior, as shown in Fig. 1(d). However, the IREE is ascribed to the interfacial Rashba effect of Bi, resulting in a constant amount of a charge current being generated via the spin conversion. Thus, the total generated charge current does not exhibit a dependence on the thickness of the Bi.

III. RESULTS AND DISCUSSION

Concerning the electric transport properties, a sharp increase in the sheet resistivity (R_{xx}) was observed with decreasing Bi thickness [see Fig. 2(a)]. Decreases in the sheet Hall coefficient ($R_H = R_{xy}/B, B = \mu_0 H$) and in the Hall mobility ($\mu_H = R_H/R_{xx}$) were also observed below 20 nm. These results indicate that the increase in R_{xx} is attributable to the decrease in μ_H, implying a significant decrease in total mobility. The absence of magnetoresistance (MR) for $\leqslant$8 nm, as shown in Fig. 2(b), also supports the behavior, because the amplitude of the MR is scaled by $\mu_H B$. The MR at 70 nm and 20 nm was analyzed using the two-carrier model of electrons and holes:

$$\frac{R_{xx}(B) - R_{xx}(0)}{R_{xx}(B)} = \frac{(N^2-1)M^2(1-M^2)\mu_H{}^2B^2}{(2M+N+NM^2)^2+(N^2-M^2)(1-M^2)\mu_H{}^2B^2}, \quad (1)$$

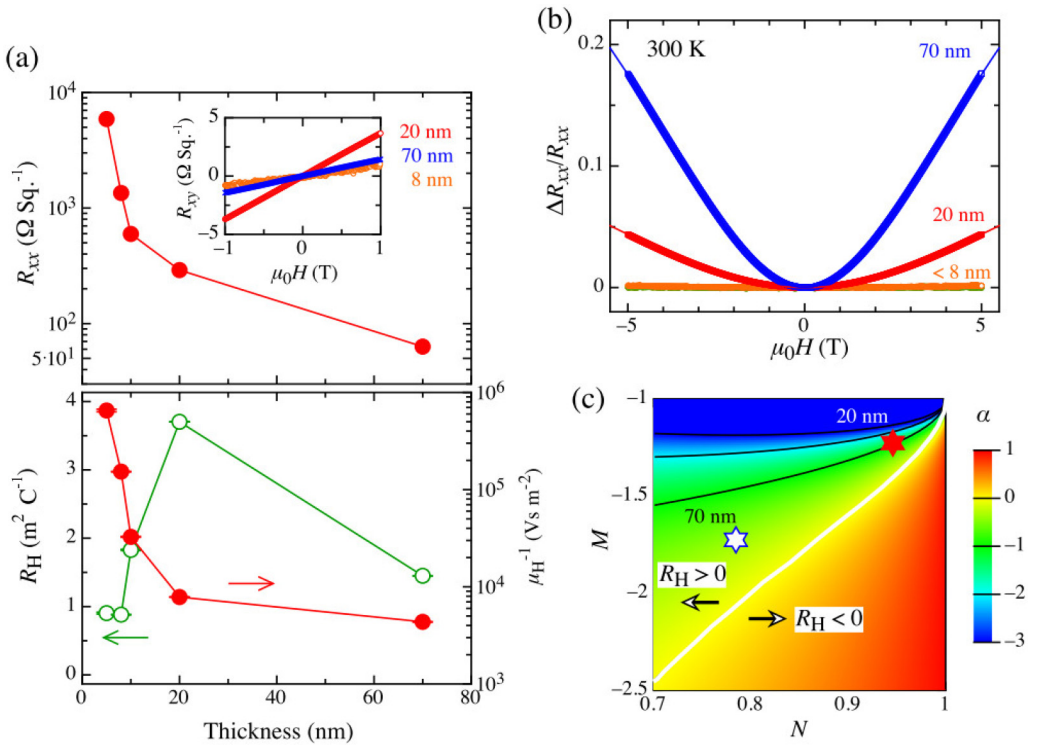

FIG. 2. (a) Thickness dependence of the sheet resistance R_{xx} of Bi/YIG at 300 K. The Hall resistance R_{xy} is shown in the inset. The thickness dependencies of the sheet Hall coefficient $R_H = R_{xy}/\mu_0 H$ and the inverse Hall mobility $\mu_H{}^{-1} = (R_H/R_{xx})^{-1}$ are also presented. (b) Magnetoresistance $[R_{xx}(H) - R_{xx}(0)]/R_{xx}(H)$ of Bi/YIG at 300 K. The fitting results using the two-carrier model are also displayed as a solid line. (c) Contour plot of Hall factor $\alpha = R_H/R_0$ determined from the two-carrier model, and the value of α determined from the magnetoresistance. The results indicate a dominance of electron conductions. See the text for details.

where n_1 and n_2 are the sheet carrier densities ($n_1 > n_2$), $N = (n_1 - n_2)/(n_1 + n_2)$, μ_1 and μ_2 are the mobilities, $M = (\mu_1 - \mu_2)/(\mu_1 + \mu_2)$, and

$$\mu_H = \frac{\mu_1 + \mu_2}{2} \cdot \beta = \frac{\mu_1 + \mu_2}{2} \cdot \frac{2M + N + NM^2}{N + M}. \quad (2)$$

Note that the value of μ_H is the experimental value, presented in the Fig. 2(a), where μ_H is $0.02302 \pm 0.000\,01\ \mathrm{m^2\,V^{-1}\,s^{-1}}$ for 70 nm, and $0.01273 \pm 0.000\,01\ \mathrm{m^2\,V^{-1}\,s^{-1}}$ for 20 nm. Furthermore, note that the mobility is defined to be negative for electrons and positive for holes. The MR was thus determined based on the two active parameters, namely, N and M, resulting in $N = 0.7848 \pm 0.0003$ and $M = -1.7250 \pm 0.0008$ for 70 nm, and $N = 0.9583 \pm 0.0001$ and $M = -1.1992 \pm 0.0002$ for 20 nm. Within the model, the sheet Hall coefficient, R_H, is expressed as

$$R_H = R_0 \cdot \alpha = R_0 \frac{2M + N + NM^2}{(N + M)^2}, \quad (3)$$

where $R_0 = [(n_1 + n_2)q_1]^{-1}$ and $q_1 = \pm e$ is the charge of the majority carrier (n_1). Here, the positive or negative charge is determined from the relation

$$\frac{\mu_1 - \mu_2}{2} = \frac{\mu_1 + \mu_2}{2} \cdot M, \quad (4)$$

because the value becomes negative for $q_1 = -e$ and positive for $q_1 = +e$. For the present case, the values were -0.1132 for 70 nm and -0.0593 for 20 nm; thus $q_1 = -e$. The majority carrier was an electron, which is the central result of the measurement. The contour plot of the Hall factor α and the value determined from N and M are shown in Fig. 2(c). The Hall factor α exhibited negative values and was consistent with the observed positive R_H values. Finally, from the experimentally determined parameters R_H,μ_H,N, and M, the two-carrier transport-related values were determined as $n_1 = [(1.43 \pm 0.02) \times 10^{18}]/\mathrm{m^2}$, $n_2 = [(0.18 \pm 0.02) \times 10^{18}]/\mathrm{m^2}$, $\mu_1 = [-(0.047 \pm 0.002)]\ \mathrm{m^2\,V^{-1}\,s^{-1}}$, and $\mu_2 = [(0.179 \pm 0.002)]\ \mathrm{m^2\,V^{-1}\,s^{-1}}$ for 70 nm, and $n_1 = [(1.76 \pm 0.03) \times 10^{18}]/\mathrm{m^2}$, $n_2 = [(0.04 \pm -0.03) \times 10^{18}]/\mathrm{m^2}$, $\mu_1 = [-(0.0099 \pm 0.0010)]\ \mathrm{m^2\,V^{-1}\,s^{-1}}$, and $\mu_2 = [(0.1088 \pm 0.0010)]\ \mathrm{m^2\,V^{-1}\,s^{-1}}$ for 20 nm. Further details of the transport measurements are provided in the Supplemental Material [20].

To understand the spin conversion properties at the Bi/YIG interface, spin pumping experiments were implemented. FMR signals from the YIG at $\theta_H = 0$ and 180 degrees were clearly found when the resonant field was 245 mT [see Fig. 3(a)]. Electromotive forces from the Bi under FMR were observed at $\theta_H = 0$ and 180 degrees, where the polarity of the signal was reversed [see Fig. 3(b)]. Because a thermally induced signal can be superimposed in the signals, we took an average of both signals [the black solid line in Fig. 3(c)]. The power dependence of the averaged electromotive forces is shown in Figs. 3(c) and 3(d), and a linear dependence was observed. These findings are in good accordance with the physical features expected in the ISHE and the IREE. The polarity of the electromotive forces due to the spin conversion indicates that the spin carrier is an electron in

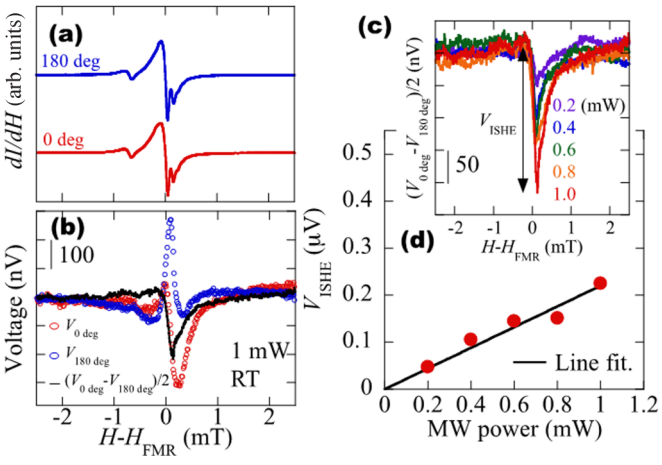

FIG. 3. (a) FMR spectra of YIG when the external magnetic field is set to be 0 (red solid line) and 180 (blue solid line) degrees, respectively. The microwave power was 1 mW. (b) Electromotive forces from Bi (20 nm)/YIG under FMR of the YIG. Red and blue open circles are experimental data at a magnetic field of 0 and 180 degrees, respectively. To subtract the thermal effect, the data are averaged (shown as a black solid line). (c, d) Excitation power dependence of the electromotive forces from Bi/YIG. The data are well fitted to a linear function.

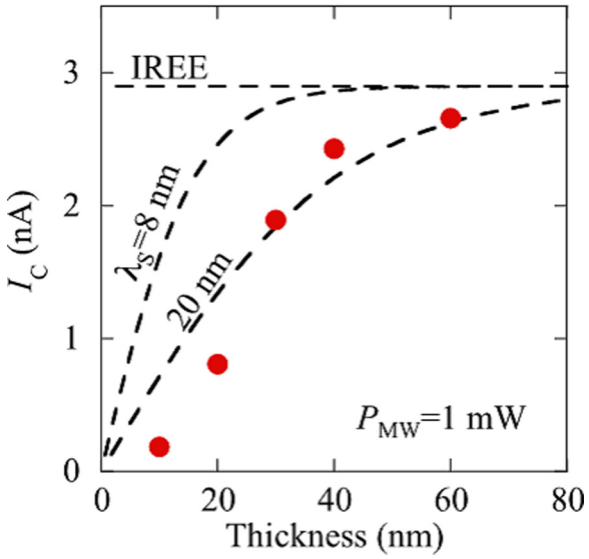

FIG. 4. Thickness dependence of the generated charge current in Bi/YIG. A monotonic increase in the charged current is clearly observed, indicating the lack of the IREE. The dashed lines labeled "IREE," "$\lambda_s = 8$ nm," and "20 nm," are the theoretical lines when we assume that the generation of the charge current is due to the IREE, the ISHE (where the spin diffusion length of the Bi is 8 nm), and the ISHE (where its spin diffusion length is 20 nm), respectively. The line "IREE" is a line assuming a certain IREE length scale.

all cases, which is consistent with the result of the transport measurement.

To reveal the physical origin of the observed signals, the thickness dependence of the electromotive forces from the Bi was investigated. Note that the spin conversion mechanisms of the ISHE and the IREE are essentially different. Because the interfacial Rashba SOI generates the IREE, a charge current converted from a pumped spin current does not depend on the Bi thickness. By contrast, the bulk SOI of Bi induces the ISHE; thus, the charge current increases along with the Bi thickness, as mentioned in Section II. The thickness dependence of the charge current (from 10 to 60 nm) is presented in Fig. 4. As shown in the figure, the charge current monotonically increased as a function of the Bi thickness, which is apparently different from the behavior expected from the IREE. The power dependence and the angular dependence of the electromotive forces are certainly consistent with the characteristics of the ISHE. Therefore, we conclude that the spin conversion in Bi/YIG, where the electromotive forces are not generated from a spin source, is attributed to the ISHE. The charge current as a function of the Bi thickness is described as

$$I_c = w\theta_{\mathrm{SHA}}\left(\frac{2e}{\hbar}\right)\lambda_s \tanh\left(\frac{d}{2\lambda_s}\right)J_s^0, \tag{5}$$

where w is the width of the Bi thin film (1.5 mm), d is the thickness of the Bi, e is the electric charge, $\hbar$ is the Dirac constant, λ_s is the spin diffusion length of the Bi, J_s^0 is the spin current density, and θ_{SHA} is the conversion efficiency of a spin current to a charge current, i.e., the spin Hall angle [26]. We performed a theoretical fitting of the experimental data by setting λ_s as a free parameter under a simple assumption that the spin diffusion length in the Bi thin films is identical. As shown in Fig. 4, the magnitude of the charge current, I_c, is consistent with Eq. (1). The spin diffusion length was estimated to be approximately 20 nm at RT under the assumption. Since the typical grain size of the Bi was measured to be several hundreds of nanometers, the spin diffusion length estimated is much smaller than the grain size. In a previous study, the spin diffusion length of Bi on NiFe was estimated to be 8 nm [13]; however, the present data cannot be explained if the spin diffusion length is 8 nm (see Fig. 4). The discrepancy is attributable to the difference in the film qualities, i.e., polycrystalline in this study and amorphous in the previous study. Here, note that the Bi thickness dependence of the generated charge current cannot be explained by the IREE, even when the spin diffusion length varies as a function of the Bi thickness. Hence, the central claim of this study, i.e., that the ISHE is dominant in the spin conversion in the Bi, is supported by the experimental results.

Finally, we briefly mention the spin Hall angle and a possible type of spin-orbit interaction in Bi. In the theoretical fitting, the spin Hall angle was estimated to be 0.000 12 for the sample with $d = 60$ nm from Eq. (1) (the spin current density was estimated to be $2.89 \times 10^{-10}\,\mathrm{J\,m^{-2}}$ for the sample; see also the Supplemental Material [20]), and this is much smaller than that of Pt (0.1 [21]), although the spin-orbit interaction of Bi is in principle twice as large as that of Pt. In previous studies, the spin Hall angle of Bi was comparatively large (0.02 [13]), the Bi was amorphous-like, and the resistivity was one order of magnitude larger than that in the Bi of this study. The disorder in the amorphous Bi easily induced the Elliot-Yafet spin relaxation. The ISHE is a spin-dependent

scattering phenomenon due to momentum scattering centers; i.e., momentum relaxation induces the ISHE. Hence, the transporting spins in the amorphous Bi are conserved by momentum relaxation through a charge current by the ISHE before they lose their spin coherence via SOI. The small spin Hall angle of the polycrystalline Bi may be attributed to the D'yakonov-Perel-type SOI originated from the heavy mass of Bi. If transporting spin angular momenta in the Bi were lost as a result of the D'yakonov-Perel-type SOI (not the momentum relaxation), the total amount of spins converted to a charge current by the ISHE in the Bi of this study would be much smaller than that in the amorphous Bi, because the spin relaxation would take place before momentum scattering occurs. This could induce a decrease in the total amount of a charge generated by the ISHE, resulting in the small spin Hall angle in the Bi. Because it is significant which type of SOI, the Elliot-Yafet or the D'yakonov-Perel, is dominant in Bi, further study is important for precise understanding of spin conversion physics in Bi.

IV. SUMMARY

In summary, we investigated the transport properties of multicarriers in thin-film semimetallic Bi that strongly govern spin conversion in the film. As measured, the electron is the dominant carrier in Bi at RT, which is consistent with the polarity of the electromotive force from the Bi observed in the spin conversion experiments. The Bi thickness dependence on the electric current generated by spin pumping and spin conversion in the Bi tells us that the spin conversion physics is governed by the ISHE, not by the IREE. This study provides significant materials for further understanding of the spin conversion physics of semimetal systems.

ACKNOWLEDGMENTS

This work was partly supported by a Grant-in-Aid for Scientific Research on Innovative Areas, "Nano Spin Conversion Science" (Grant No. 26103003) and by a Grant-in-Aid for Scientific Research (A) (Grant No. 15H02108).

[1] A. V. Ettingshausen and W. Nernst, Ann. Phys. **265**, 343 (1886).
[2] L. Schubnikov and W. J. de Haas, Comm. Phys. Lab. Leiden **207d**, 35 (1930).
[3] W. J. de Haas and P. M. van Alphen, Comm. Phys. Lab. Leiden, **212a**, 3 (1930).
[4] T. J. Seebeck, Abh. Akad. Wiss. Berlin **289** (1821).
[5] M. S. Dresselhaus, J. Phys. Chem. Solids **32**(Suppl. 1), 3 (1971).
[6] M. H. Cohen and E. I. Blount, Philos. Mag. **5**, 115 (1960).
[7] P. A. Wolff, J. Phys. Chem. Solids **25**, 1057 (1964).
[8] Y. Liu and R. E. Allen, Phys. Rev. B **52**, 1566 (1995).
[9] D. Shoenberg and M. Z. Uddin, Proc. R. Soc. London A **156**, 687 (1936).
[10] Y. Yafet, *Solid State Physics*, 5th ed., Vol. 14 (Academic Press, NY, 1963).
[11] D. Hou, Z. Qiu, K. Harii, Y. Kajiwara, K. Uchida, Y. Fujikawa, H. Nakayama, T. Yoshino, T. An, K. Ando, X. Jin, and E. Saitoh, Appl. Phys. Lett. **101**, 042403 (2012).
[12] H. Emoto, Y. Ando, E. Shikoh, Y. Fuseya, T. Shinho, and M. Shiraishi, J. Appl. Phys. **115**, 17C507 (2014).
[13] J.-C. Rojas-Sánchez, L. Villa, G. Desfonds, S. Gambarelli, J. P. Attané, J. M. De Teresa, C. Magén, and A. Fert, Nat. Commun. **4**, 2944 (2013).
[14] V. M. Edelstein, Solid State Commun. **73**, 233 (1990).
[15] G. Eguchi, K. Kuroda, K. Shirai, Y. Ando, T. Shinjo, A. Kimura, and M. Shiraishi, Phys. Rev. B **91**, 235117 (2015).
[16] C. R. Ast, J. Henk, A. Ernst, L. Moreschini, M. C. Falub, D. Pacile, P. Bruno, K. Kern, and M. Grioni, Phys. Rev. Lett. **98**, 186807 (2007).
[17] A. Tsukahara, Y. Ando, Y. Kitamura, H. Emoto, E. Shikoh, M. P. Delmo, T. Shinjo, and M. Shiraishi, Phys. Rev. B **89**, 235317 (2014).
[18] L. Chen, S. Ikeda, F. Matsukura, and H. Ohno, Appl. Phys. Express **7**, 013002 (2014).
[19] S. Mizukami, Y. Ando, and T. Miyazaki, Phys. Rev. B **66**, 104413 (2002).
[20] See Supplemental Material at http://link.aps.org/supplemental/10.1103/PhysRevB.93.174428 for detailed transport properties of the Bi and physical parameters for estimating the spin current density.
[21] H. L. Wang, C. H. Du, Y. Pu, R. Adur, P. C. Hammel, and F. Y. Yang, Phys. Rev. Lett. **112**, 197201 (2014).